



Deposited via The University of Leeds.

White Rose Research Online URL for this paper:

<https://eprints.whiterose.ac.uk/id/eprint/91058/>

Version: Accepted Version

Article:

Corbi, F, Rivalta, E, Pinel, V et al. (2015) How caldera collapse shapes the shallow emplacement and transfer of magma in active volcanoes. *Earth and Planetary Science Letters*, 431. 287 - 293. ISSN: 0012-821X

<https://doi.org/10.1016/j.epsl.2015.09.028>

© 2015. This manuscript version is made available under the CC-BY-NC-ND 4.0 license
<http://creativecommons.org/licenses/by-nc-nd/4.0/>

Reuse

Items deposited in White Rose Research Online are protected by copyright, with all rights reserved unless indicated otherwise. They may be downloaded and/or printed for private study, or other acts as permitted by national copyright laws. The publisher or other rights holders may allow further reproduction and re-use of the full text version. This is indicated by the licence information on the White Rose Research Online record for the item.

Takedown

If you consider content in White Rose Research Online to be in breach of UK law, please notify us by emailing eprints@whiterose.ac.uk including the URL of the record and the reason for the withdrawal request.

How caldera collapse shapes the shallow emplacement and transfer of magma in active volcanoes

Authors: F. Corbi^{1*}, E. Rivalta¹, V. Pinel², F. Maccaferri¹, M. Bagnardi³, V. Acocella⁴

Affiliations:

¹GFZ German Centre for Geosciences, Section 2.1, Telegrafenberg, 14473 Potsdam, Germany.

²ISTerre, Université Savoie Mont-Blanc, IRD, CNRS, Campus Scientifique, Le Bourget du Lac F73376, France.

³COMET, School of Earth and Environment, University of Leeds, Leeds LS2 9JT, UK.

⁴Dipartimento di Scienze, University of Roma Tre, L. S.L. Murialdo, 1, 00146, Rome, Italy.

*Correspondence to: fabio.corbi@gfz-potsdam.de.

Abstract: Calderas are topographic depressions formed by the collapse of a partly drained magma reservoir. At volcanic edifices with calderas, eruptive fissures can circumscribe the outer caldera rim, be oriented radially and/or align with the regional tectonic stress field. Constraining the mechanisms that govern this spatial arrangement is fundamental to understand the dynamics of shallow magma storage and transport and evaluate volcanic hazard. Here we show with numerical models that the previously unappreciated unloading effect of caldera formation may contribute significantly to the stress budget of a volcano. We first test this hypothesis against the ideal case of Fernandina, Galápagos, where previous models only partly explained the peculiar pattern of circumferential and radial eruptive fissures and the geometry of the intrusions determined by inverting the deformation data. We show that by taking into account the decompression due to the caldera formation, the modeled edifice stress field is consistent with all the observations. We then develop a general model for the stress state at volcanic edifices with

calderas based on the competition of caldera decompression, magma buoyancy forces and tectonic stresses. These factors control: 1) the shallow accumulation of magma in stacked sills, consistently with observations; 2) the conditions for the development of circumferential and/or radial eruptive fissures, as observed on active volcanoes. This top-down control exerted by changes in the distribution of mass at the surface allows better understanding of how shallow magma is transferred at active calderas, contributing to forecasting the location and type of opening fissures.

Keywords: caldera collapse, decompression, dike propagation, Finite Element model, Fernandina

1. Introduction

The dynamics of magma storage, transport and eruption are thought to be controlled by both bottom-up (e.g., magma supply rate, volume and composition; e.g., Poland et al., 2012; Galland et al., 2014) and top-down processes (e.g., the effect of edifice load on magma ascent; e.g., Pinel and Jaupart, 2000; Muller et al., 2001). Understanding the state of stress within a volcanic edifice is one of the key ingredients to improve our ability of forecasting magma propagation and eruption. Most polygenetic volcanoes are formed over long time scales by deposition and compaction of volcanic products that create a time-evolving stress state within the edifice. The stress field may be later modified by diffuse fracturing, diking or redistribution of surface mass (e.g. landslides), and by changes in the mechanical properties of the rock layers themselves as the layers tend to become stiffer with time. The simple assumption of a gravitationally loaded volcano may, therefore, be very far from reality for most volcanoes around the world. Important clues into the stress state of a volcano come from the orientation of dikes and fissures observed in the field, as they tend to orient perpendicularly to the direction of the minimum compressive stress, σ_3 (Anderson, 1951) and be controlled by stress gradients (buoyancy, edifice and regional stresses).

Calderas are sub-circular topographic depressions created by the yielding of a magma chamber, drained by large intrusions, effusive or explosive eruptions (Lipman 2000; Cole et al., 2005). Post-caldera volcanism is commonly fed by regional, circumferential and radial dikes (e.g., Acocella and Neri, 2009). Regional dikes are often sub-vertical and aligned orthogonal to the regional tectonic σ_3 , as observed along the axis of rift zones, both within and outside the calderas. Dikes that propagate within the volcanic edifice are likely to be controlled by the local stress field (Gautneb and Gudmundsson, 1992). These dikes may be arranged as centrally-inclined sheets (e.g., cone sheets), which are commonly circular or elliptical in map view, and/or have a radial distribution in alignment with the axis of the edifice (e.g., Acocella and Neri, 2009). Although their orientation at the surface may mimic that of ring faults (i.e., shear fractures), inclined sheets are magma-filled extensional fractures. Both radial dikes and inclined sheets have been observed at several eroded volcanoes, with the latter also possibly associated to shallow viscous magma (Galland et al., 2014). In particular, inclined sheets have been identified in Scotland (e.g. Burchardt et al., 2013), the Canary Islands (e.g., Ancochea et al., 2003), Japan (Geshi, 2005), and Iceland (e.g. Burchardt and Gudmundsson, 2009). Their surface expression as circumferential eruptive fissures is, on the other hand, relatively rare, and has only been observed around calderas in the western Galápagos Archipelago (Fernandina, Wolf, Darwin, Alcedo, Sierra Negra and Cerro Azul; Chadwick and Howard, 1991) and, to lesser extent, in Iceland at Krafla, Grimsvotn (Thordarson and Self, 1993) and Askja calderas (Hartley and Thordarson, 2012), Dolomieu (Piton de la Fournaise, La Réunion; Carter et al., 2006), Rano Kau (Easter Island; Vezzoli and Acocella, 2009); and other planets (Venus, Tharsis Province on Mars; e.g., Montési, 2001) calderas. The rare and selective distribution of circumferential eruptive fissures suggests that most inclined sheets stall at depth, without reaching the surface, and that formation of these fissures is favored, but not guaranteed, by the presence of a caldera. This may imply a specific stressing mechanism active at volcanoes with a caldera, competing with other stressing factors.

Some of the best-developed circumferential fissures are found at Fernandina (Galápagos; Fig1; Chadwick and Howard, 1991), which hosts a ~1 km deep and ~6.5 x 4 km wide caldera resulting from several collapses testified by old benches and a ~350 m drop of the SE caldera floor in

1968 (Simkin and Howard, 1970; Howard, 2010). Several models have been proposed to explain the formation of circumferential fissures at Fernandina, considering the effect of: a) caldera faults capturing and channeling magma to the caldera rim (Nordlie, 1973, Browning and Gudmundsson, 2015); b) caldera walls unbuttressing re-orienting the minimum compressive stress perpendicular to them (Simkin, 1984; Munro and Rowland 1996); c) stress perturbations due to the pressurization of a magma chamber (Chadwick and Dieterich, 1995; Chestler and Grosfils, 2013) or d) a previous intrusion (Bagnardi et al., 2013). The caldera fault model was excluded based on observing: i) no displacement in layers adjacent to circumferential dikes; ii) circumferential dikes crosscutting caldera faults; and iii) circumferential fissures located well downslope from the caldera rim (Chadwick and Dieterich, 1995). The edifice unbuttressing model fits well with the orientation of circumferential fissures at the surface but is inconsistent with intrusions starting as sills (Chadwick et al., 2011; Bagnardi et al., 2013). The most accredited models now appeal to the inflation of magma reservoirs of various shapes. For example, the inflation of a diapir-shaped source plus the uniform surface load due to the emplacement of lava flows applied from the caldera wall outward produce a stress field consistent with proximal circumferential dikes and distal radial dikes (Chadwick and Dietrich, 1995).

Recent crustal deformation studies have revealed previously unknown features of magma transport beneath Fernandina. Modeling of InSAR data showed that the dike feeding the 2005 eruption started as a sub-horizontal sill that curved upward and erupted through proximal circumferential fissures (Chadwick et al., 2011; Bagnardi et al., 2013). The magma injection feeding the subsequent 2009 eruption also started as a sub-horizontal sill that, propagating laterally, turned into a dike with dip angle increasing from 33° to 50°, indicating a progressive twisting about a radial axis (Bagnardi et al., 2013). Radial fissures present on the volcano flanks result therefore from shallow dipping dikes intersecting the volcano topography (Jónsson et al., 1999; Bagnardi et al., 2013). While former interpretations and models on the mechanics of magma transport were constrained only by the eruptive fissure distribution at the surface, current robust constraints on the 3D sub-surface intrusion geometry now allow us to test previous and new models.

Analytical and numerical models of local stresses around magma chambers have been used to infer dike propagation paths to the surface, as well as their arrest at depth (e.g., Gudmundsson 2006). Chestler and Grosfils (2014) calculated the stress pattern due to the inflation of an oblate reservoir, as there is a widespread geological, geophysical and modeling evidence that these are the most common shapes for magma reservoirs (e.g., Petford et al., 2000). The authors focus on the conditions necessary to generate radial dikes, inclined sheets and sills twisting into radial dikes based on rupture orientation at the chamber wall as well as orientation of σ_3 within the edifice with specific application to Fernandina. This study revealed that radial dikes can initiate at the reservoir wall only for mildly oblate reservoirs (with aspect ratio around 1.3) however such reservoirs are difficult to reconcile with the flat-topped reservoir geometry imaged for Fernandina (Chadwick et al., 2011; Bagnardi and Amelung, 2012). For more oblate reservoirs (i.e., aspect ratio >2), intrusions are expected to initiate as sills at the chamber wall. Then depending on the chamber aspect ratio and based on the orientation of σ_3 , different magma paths and dike geometries are derived but none of them is consistent either with a sill bending into an upward propagating dike (with an upward concavity) to feed a circumferential fissure or with a radially propagating dike reaching the surface in the flank area, since σ_3 is always in plane in the upper 1.5 – 2.0 km beneath the surface. Moreover, magma reservoirs depressurize while injecting a sill or a dike (e.g., Gudmundsson, 2006) reducing the magnitude of the induced stress perturbation. Simultaneously, as the dikes elongate the stress concentration at their tip will intensify, resulting in a decrease of the role played by the other contributions (magma chamber or unloading).

The orientation and location of the eruptive fissures at Fernandina was related to the stress perturbation from earlier intrusions (Bagnardi et al., 2013). For example, the 2005 intrusion was found consistent with the stress perturbation due to the intrusion of a sill with geometry, location and displacement derived for the preceding 1995 intrusion. This model may explain both the location and orientation of the fissures and the alternation between circumferential and radial fissures observed recently (i.e., circumferential in 1982, radial in 1995, circumferential in 2005, and radial in 2009), but provides a mechanism that can only be tested at Fernandina.

Here we propose that the gravitational unloading due to surface mass redistribution associated with the formation of a caldera may contribute significantly to the stress budget within a volcanic edifice. Collapses may lower the caldera floors by several hundreds meters up to a few km, so that a large decompression of the magmatic system (~ 8 MPa for 300 m of collapse) may occur in a relatively short time interval. Such decompression may dominate over tectonic stresses and magma chamber pressurizations. Topographic effects have been previously considered as a notch in the morphology. Such notches concentrate stresses around them and are found to influence dike propagation only at very shallow levels (few tens of m to few hundreds m; e.g., Gudmundsson, 1998; Gudmundsson, 2011), while gravitational unloading due to the removal of mass from the surface may lead to significant rotation of the principal stresses and affect the dynamics of magma propagation also at deeper levels (Hooper et al., 2011; Maccaferri et al., 2014). We test this possibility using numerical Finite Element (FE) models to calculate the stress field within a volcanic edifice decompressed during the formation of a caldera and investigate the expected orientation of the magma intrusions.

2. Methods

We use the COMSOL Multiphysics® software based on the Finite Element method to generate a series of models assuming a homogeneous elastic medium with 2D axisymmetric configuration. We use a 100 x 100 km² model shaped accordingly to the average topography of Fernandina extracted from the SRTM VERSION 2_1 DEM and the NGDC-NOAA bathymetry offshore W Fernandina. The properties of the subdomains are set as follows: density $\rho=2700$ kg·m⁻³, Poisson's ratio $\nu=0.25$ and shear modulus $G=10$ GPa. The bottom and lateral boundaries are set as zero normal displacement. The model's surface is set as free.

As for the reference stress state of the volcano over which to superpose the stress perturbation, we assume an initially isotropic reference stress field (e.g., Chadwick and Dieterich, 1995; Bagnardi et al., 2013). This is justified by the slow and gradual growth of the volcano, by repeated injection of dikes homogenizing the stress, and by diffuse fracturing that would continuously release the deviatoric stresses by inelastic deformation. Unloading is simulated by

applying a vertical tensile stress on the caldera floor and steep caldera walls, assuming that in the pre-caldera stage there was a flat surface at the elevation of the caldera rim, $H_c=1290$ m. The amount of unloading, U , is calculated as $U=\rho \cdot g \cdot (H_c-H_t)$; where H_t is the elevation of each point along the caldera profile.

The stress field in the volcano after collapse may be rather complicated, with a stress arch in the roof of the magma chamber, stress concentrations and shear/tensile failure (Holohan et al., 2015). We do not model caldera collapse as such. A quantitative estimation of stresses coming from the collapse itself would depend on different collapse structural styles and apply only to specific cases. For this reason, we focus on the decompression stresses acting below the caldera area of a volcano due to mass redistribution. Complications like caldera bounding faults are also neglected because: a) at Fernandina the eruptive activity is located well outside of the ring fault margins (Chadwick and Dieterich, 1995); b) the decompression due to the formation of a 1000 m deep caldera is expected to dominate over other processes such as faulting, that cause localized stress concentrations and are capped by the shear or tensile strength of rock; c) the stress variation depends on the geometry and dip of the faults; inward- and outward-dipping faults will have opposite effects. Moreover, we do not include the stress perturbations due to a pressurized reservoir or previous intrusions. We will rather infer as a result of our model the favored shape and orientation of a reservoir forming in response to the modeled stress conditions.

3. Results

We find that added to an isotropically stressed volcano, gravitational unloading induces a complex stress rotation. σ_3 is in plane sub-vertical beneath the caldera region and rotates progressively to sub-horizontal moving toward the sides of the edifice (Fig.2a). σ_3 becomes out of the axisymmetric plane at shallow depth below the volcano flanks, in a region that is ~ 2 km deep at the coastline and tapering towards the summit plateau.

Intrusions fed by a shallow magma reservoir (~ 1 km b.s.l.) are expected to initiate horizontally as sills that steepen progressively during their lateral propagation and erupt on the summit plateau. Along such path σ_3 lies on the axisymmetric plane, except for the uppermost ~ 500 m where it

becomes out of plane; therefore fissures are expected to be primarily circumferential, with minor deviations e.g. the 1958 fissure at Fernandina (Chadwick and Howard, 1991).

Intrusions originating from deeper regions (>2 km b.s.l.) are also expected to start as sills that progressively bend upward, but they encounter a wide region where σ_3 is perpendicular to the axisymmetric plane (i.e., tangential) and the maximum compressive stress σ_1 is radial sub-horizontal, promoting radial dikes. These dikes are forced to twist about an axis parallel to the direction of propagation and feed radial fissures, as in 1995 and 2009 (Jónsson et al., 1999; Bagnardi et al., 2013). The length-scale over which a complete 90° twist occurs will depend on dike overpressure and the magnitude of the deviatoric stress and its gradient, and is inferred to occur beneath off-shore rifts to the W of Fernandina (Bagnardi et al., 2013).

We also test the case of a gravitationally loaded volcano. We added a body load to a pre-stressed edifice under lithostatic (isotropic) conditions (e.g., Chestler and Grosfils, 2013). This results in pervasive vertical σ_1 , with only minor deflection (few degrees) in the sub-caldera rock volume. In fact the effect of the volcanic edifice sagging under its own weight is much larger than the caldera missing load (Fig.2b). σ_3 is in plane and sub-horizontal in most of the sub-caldera region and out of plane along the volcano flanks. This configuration would therefore be consistent with vertical proximal circumferential dikes and distal radial dikes, but not with the intrusion initiation as sill and the upward bending observed during the recent intrusions. Moreover, this model is not compatible with the flat-topped magma chamber imaged for Fernandina (Chadwick et al., 2011; Bagnardi and Amelung, 2012), since the sub-horizontal σ_3 would not favor horizontal magma propagation.

4. Discussion

4.1 Unloading pressure vs. dike overpressure control on the eruptive fissure distribution of Fernandina and other calderas

Our FE model demonstrates that the unloading effect generated by caldera formation explains the sub-surface intrusion geometry linked to the last three eruptions at Fernandina, including the

initial sill propagations and the following bending or twisting. This geometry cannot be explained when considering a stress field resulting from a gravitationally loaded edifice in the absence of stress relaxation. Similar cone sheet geometries, albeit without the characteristic twisting observed at Fernandina, have been also experimentally obtained with shallow intrusions, depending on the geometrical configuration of the system and the dynamic interplay between host-rock properties and viscous stresses (Galland et al., 2014).

Our calculation, in line with previous studies for Fernandina, is static, as we do not simulate the dike propagation. We simply assume that the dikes propagate orthogonal to σ_3 . Numerical models of dike propagation (Dahm, 2000; Maccaferri et al., 2011) and analog experiments (Watanabe et al., 2002) revealed that dike trajectories depend on the competition between dike overpressure and the external stresses (i.e., loading or unloading). High-overpressure dikes are expected to propagate straight, insensitive to spatial inhomogeneities of the stress field. Low-overpressure dikes follow closely the trajectories perpendicular to σ_3 . Available numerical models for the trajectory followed by dikes are only 2D, so that it is difficult to estimate quantitatively the distance needed by a dike to twist and align perpendicular to σ_3 .

Analog experiments addressed this issue for the case of dike bending, demonstrating that when the ratio between loading pressure (or equivalently unloading), P_l , and dike overpressure, P_e , is larger than 5, the dikes propagate closely orthogonal to σ_3 (Watanabe et al., 2002). $P_l = \rho g H$, where ρ is the density of rock, g is the acceleration due to gravity, and H is the observed caldera depth at present. P_l therefore does not take into account the modality of collapse (incremental or single collapses), as the amount of unloading affects only the magnitude of stresses and not the principal component orientation. $P_e = \Delta \rho g L_z / 4$, where L_z is the projection of the dike length on the vertical axis and $\Delta \rho$ the density contrast between solid host rocks and magma. Since here we are not concerned with the nucleation process of the dikes but only with their propagation path once they have already formed, we simplify the problem by neglecting the stresses of the just decompressed chamber. For this reason P_e must be considered as a conservative estimation of magma driving force.

We consider these results and test whether Fernandina, together with 14 of the best-studied calderas worldwide, satisfy the $PI/Pe > 5$ condition, leading to intrusions propagating closely orthogonal to σ_3 . We assume that the magma chamber depth is a proxy for L_z and that dikes do not get arrested on their way to the surface. The derived PI/Pe is therefore a conservative estimate. For Fernandina we obtain $PI/Pe = 13-119$ (with $\Delta\rho$ of $100-300 \text{ kg}\cdot\text{m}^{-3}$, L_z between $1000 - 3000 \text{ m}$ and $H = 1100 \text{ m}$), indicating that the unloading of the caldera is strong enough to deviate effectively most dikes. If instead of the full caldera depth, only the last event is considered (i.e., $H = 350 \text{ m}$), the stress pattern remains unchanged as expected due to linearity of equations of elasticity and $PI/Pe = 4-38$ for the same parameters as above. Similar orientations of the principal stresses are also obtained for the other western Galápagos volcanoes with slightly smaller PI/Pe (between 7 and 23). Here the magnitude of unloading is smaller due to the shallower calderas (table ST1). These ratios are therefore consistent with the deviations in the pattern of circumferential and radial fissures across the Galápagos volcanoes, and in particular with the more developed pattern of fissures around the deeper Fernandina caldera.

We measured the cumulative length of circumferential fissures relative to that of radial ones, C/R , at several calderas worldwide as a function of PI/Pe (Fig. 3). C/R assumes that the burial probability from previous eruption is the same for circumferential and radial fissures. Calderas with more prominent unloading, least density contrast between magma and host rock, and shallowest magma reservoir develop circumferential fissures, as for example Fernandina (top right). Conversely, calderas with minor collapsed volume (including those filled by post-collapse deposits or water), more buoyant magma and deeper reservoir do not show any circumferential fissure, as Toba, (bottom left). In between, lie calderas with intermediate features, as Tambora, with still prominent unloading but also with deeper reservoirs and gas-rich buoyant magma that limits the propagation of any circumferential dike.

In the total edifice stress budget, local and regional tectonic stresses should also be considered.

While tangential dikes (as cone sheets) have been found in various tectonic settings, all calderas surrounded by circumferential fissures (with the exception of Oskjuvatn) are characterized by hot-spot volcanism. Therefore the influence of regional stresses can be considered negligible

compared to other volcanoes close to plate boundaries. A horizontal regional stress of 5-10 MPa (e.g., Buck et al., 2006; Maccaferri et al., 2014) in extensional or compressional domains would be sufficient to effectively mask the stress field caused by caldera unloading and favor the pervasive emplacement of vertical dikes and sills, respectively. Given its intra-plate location, Fernandina lacks significant regional control and the role of unloading stresses dominates.

We conclude that considering the total stress budget as a sum of correctly estimated edifice stresses, buoyancy and regional stresses, explains the pattern of circumferential and radial eruptive fissures at several calderas worldwide. This stress budget also explains why only very few circumferential eruptive fissures on active volcanoes are fed from the widespread cone sheets at depth within eroded volcanoes.

4.2 Caldera collapse control on the magma plumbing system

The formation of a caldera will affect the dynamics of the magma plumbing system. Initially, the stress gradient due to caldera collapse promotes the rise of magma (Fig.4a). In general, this may lead to post-caldera resurgence (Kennedy et al., 2012) and/or increased volcanism due to the decompression of a shallow reservoir that would favor the rise of magma from a deeper source if the reservoirs are hydraulically connected through a magmatic plumbing system (Pinel and Jaupart, 2000; Hooper et al., 2011). In case of significant unloading ($P_l/P_e > 5$), the vertical orientation of σ_3 beneath the caldera promotes shallow, flat-topped magma bodies (Fig.4b). This could explain why flat-topped magma reservoirs are common beneath well-known calderas, including Toba (Jaxybulatov et al., 2014), Yellowstone (Chang et al., 2010), Campi Flegrei (Zollo et al., 2008), Sierra Negra (Yun et al., 2006), Fernandina (Chadwick et al., 2011; Bagnardi and Amelung, 2012), Long Valley (Liu et al., 2011), Slaufudalur (Burchardt et al., 2011) and those along the Main Ethiopian Rift (Biggs et al., 2011), and why most extinct magma reservoirs consist of sub-horizontal tabular intrusions (Petford et al., 2000; Annen, 2009).

If the thickness is enough to ensure magma mobility as the cooling process proceeds slowly, the sill may grow laterally while absorbing a large fraction of the magma that enters it (Gudmundsson, 1990). The lateral growth of sill-like reservoirs is discouraged beyond the

caldera rim (Fig.4c), where the driving force of magma is reduced (Pinel and Jaupart, 2000). Such effect is due to the caldera unloading stress and is strengthened by the loading due to the rim topography. High walls surrounding calderas act as a trap for sills, which would require higher magma overpressure to propagate and erupt, favoring magma stagnation, differentiation and creating the potential for explosive eruptions (Caricchi et al., 2014). Also caldera boundary faults may arrest the lateral propagation of sheets or deflect them vertically into the faults depending on the contrasting mechanical properties of the host rock and fault zone (Browning and Gudmundsson, 2015).

If the magma pressure within the intrusions exceeds the compressive effect exerted by the caldera rim, dikes can propagate toward the surface. The final orientation and eruption location can be forecast from their nucleation depth (Fig.4d). Shallow intrusions (with depth in the range of half the caldera diameter or shallower) feed circumferential dikes, while deeper sources feed intrusions that twist about a radial axis erupting as radial fissures.

5. Conclusions

Our model of magma storage and transport beneath calderas reveals the previously unappreciated primary role of surface mass removal in the dynamics of the shallow plumbing system. Following caldera collapse, sufficiently high unloading stresses with respect to magma overpressure (i.e., ratio greater than 5) and to regional stresses favor the development of shallow-reaching and flat-topped reservoirs (i.e., systems of stacked sills).

Dike trajectories are also controlled by the stress field imposed by unloading, by the depth at which dikes nucleate, and by the density of magma. We show that the unloading due to caldera formation applied to an isotropically stressed volcano is able to reconcile all observations on magma paths at Fernandina, and in general the presence of circumferential and/or radial eruptive fissures at worldwide volcanic edifices with calderas. In particular, we propose a model based on the competition of caldera decompression, magma buoyancy forces and tectonic stresses, which control the shallow accumulation of magma in stacked sills and the conditions to develop circumferential and/or radial eruptive fissures.

In addition to the "bottom-up" control by magma inflow, the "top-down" control by changes in the surface mass load may strongly influence the shape and volume of the magma storage system and the spatial distribution of the eruptive vents. This may contribute in forecasting the location and type of opening fissures at calderas.

References:

1. V. Acocella, M. Neri, Dike propagation in volcanic edifices: Overview and possible developments. *Tectonophysics*. **471**, 67–77 (2009).
2. E. Ancochea, J.L. Brändle, M.J. Huertas, C.R. Cubas, F. Hernan, The felsic dikes of La Gomera (Canary Islands): identification of cone sheet and radial dike swarms. *J. Volcanol. Geoth. Res.* **120**, 197-206. (2003)
3. E. M. Anderson, 1951, The dynamics of faulting and dyke formation with applications in Britain, second edition: London, Oliver and Boyd, 206 p.
4. C. Annen, From plutons to magma chambers: Thermal constraints on the accumulation of eruptible silicic magma in the upper crust. *Earth Planet. Sci. Lett.* **284**, 409–416 (2009).
5. M. Bagnardi, F. Amelung, Space-geodetic evidence for multiple magma reservoirs and subvolcanic lateral intrusions at Fernandina Volcano, Galápagos Islands. *J. Geophys. Res.* **117**, B10406 (2012).
6. M. Bagnardi, F. Amelung, M. P. Poland, A new model for the growth of basaltic shields based on deformation of Fernandina volcano, Galápagos Islands. *Earth Planet. Sci. Lett.* **377-378**, 358–366 (2013).
7. J. Biggs, I.D. Bastow, D. Keir, E. Lewi. Pulses of deformation reveal frequently recurring shallow magmatic activity beneath the Main Ethiopian Rift. *Geochem. Geophys. Geosyst.* 12/9 (2011). DOI: 10.1029/2011GC003662
8. J. Browning, A. Gudmundsson, Caldera faults capture and deflect inclined sheets: an alternative mechanism of ring dike formation. *Bull. Volcanol.* (2015), doi:10.1007/s00445-014-0889-4.
9. S. Burchardt, A. Gudmundsson, The infrastructure of Geitafell Volcano, Southeast Iceland. In: Thordarson, T., Self, S., Larsen, G., Rowland, S., Hoskuldsson, A. (eds.). *Studies in Volcanology: The Legacy of George Walker*. Special Publications of IAVCEI 2. Geological Society, London, 349-370 (2009).
10. S. Burchardt, D.C. Tanner, M. Krumbholz, 2011. Emplacement of the Slaufudalur Pluton, Southeast Iceland – An example of shallow magma emplacement by coupled cauldron subsidence and magmatic stopping. *Geol. Soc. of Am. Bull.* **124**, 213-227 (2011). doi:10.1130/B30430.1.

11. S. Burchardt, V. R. Troll, L. Mathieu, H. C. Emeleus, C. H. Donaldson, Ardnamurchan 3D cone-sheet architecture explained by a single elongate magma chamber. *Sci. Rep.* **3**, 2891 (2013).
12. L. Caricchi, C. Annen, J. Blundy, G. Simpson, V. Pinel, Frequency and magnitude of volcanic eruptions controlled by magma injection and buoyancy. *Nat. Geosci.* **7**, 126–130 (2014).
13. Carter, B. van Wyk de Vries, K. Kelfoun, P. Bachèlery, P. Briole, Pits, rifts and slumps: the summit structure of Piton de la Fournaise. *Bull. Volcanol.* **69**, 741–756 (2006).
14. W. W. Chadwick, J. H. Dieterich, Mechanical modeling of circumferential and radial dike intrusion on Galapagos volcanoes. *J. Volcanol. Geotherm. Res.* **66**, 37–52 (1995).
15. W. W. Chadwick, K. Howard, The pattern of circumferential and radial eruptive fissures on the volcanoes of Fernandina and Isabela islands, Galapagos. *Bull. Volcanol.*, 259–275 (1991).
16. W. W. Chadwick *et al.*, The May 2005 eruption of Fernandina volcano, Galápagos: The first circumferential dike intrusion observed by GPS and InSAR. *Bull. Volcanol.* **73**, 679–697 (2011).
17. W.-L. Chang, R. B. Smith, J. Farrell, C. M. Puskas, An extraordinary episode of Yellowstone caldera uplift, 2004–2010, from GPS and InSAR observations *Geophys. Res. Lett.*, **37**, L23302 (2010). doi:10.1029/2010GL045451.
18. S. R. Chestler, E. B. Grosfils, Using numerical modeling to explore the origin of intrusion patterns on Fernandina volcano, Galapagos Islands, Ecuador *Geophys. Res. Lett.*, **40**, 4565–4569 (2013). doi:10.1002/grl.50833.
19. J. W. Cole, D. M. Milner, K. D. Spinks, Calderas and caldera structures: A review. *Earth-Science Rev.* **69**, 1–26 (2005).
20. T. Dahm, Numerical simulations of the propagation path and the arrest of fluid-filled fractures in the Earth. *Geophys. J. Int.* **141**, 623–638 (2000).
21. O. Galland, S. Burchardt, E. Hallot, R. Mourgues, C. Bulois, Dynamics of dikes versus cone sheets in volcanic systems. *J. Geoph. Res.: Solid Earth* **118**, 6178–6192. (2014). doi: 10.1002/2014JB011059.
22. H. Gautneb, A. Gudmundsson, Effect of local and regional stress fields on sheet emplacement in West Iceland. *J. Volcanol. Geotherm. Res.* **51**, 339–356 (1992).
23. N. Geshi, Structural development of dike swarms controlled by the change of magma supply rate: the cone sheets and parallel dike swarms of the Miocene Otoge igneous complex, Central Japan. *J. Volcanol. Geoth. Res.* **141**, 267–281 (2005).
24. A. Gudmundsson, Emplacement of dikes, sills and crustal magma chambers at divergent plate boundaries. *Tectonophysics.* **176**, 257–275 (1990).
25. A. Gudmundsson, Formation and development of normal-fault calderas and the initiation of large explosive eruptions. *Bull. Volcanol.* **60**, 160–170 (1998).

26. A. Gudmundsson, How local stresses control magma-chamber ruptures, dyke injections, and eruptions in composite volcanoes. *Earth-Science Rev.* **79**, 1–31 (2006).
27. A. Gudmundsson, 2011. *Rock Fractures in Geological Processes*. Cambridge, Cambridge University Press.
28. M. E. Hartley, T. Thordarson, Formation of Öskjuvatn caldera at Askja, North Iceland: Mechanism of caldera collapse and implications for the lateral flow hypothesis. *J. Volcanol. Geotherm. Res.* **227-228**, 85–101 (2012).
29. E. Holohan, M. Schöpfer, J. Walsh, Stress evolution during caldera collapse : a Distinct Element Method perspective. *Earth Planet. Sci. Lett.* **15**, 2208 (2015).
30. A. Hooper *et al.*, Increased capture of magma in the crust promoted by ice-cap retreat in Iceland. *Nat. Geosci.* **4**, 783–786 (2011).
31. K. Howard, Caldera collapse: Perspectives from comparing Galápagos volcanoes, nuclear-test sinks, sandbox models, and volcanoes on Mars. *GSA Today.* **20**, 4–10 (2010).
32. K. Jaxybulatov, N. M. Shapiro, I. Koulakov, A. Mordret, A large magmatic sill complex beneath the Toba caldera. *Science.* **346**, 617 (2014). DOI: 10.1126/science.1258582
33. S. Jónsson, H. Zebker, P. Cervelli, A shallow-dipping dike fed the 1995 flank eruption at Fernandina Volcano, Galápagos, observed by satellite radar interferometry. *Geophys. Res.* **26**, 1077–1080 (1999).
34. B. Kennedy, J. Wilcock, J. Stix, Caldera resurgence during magma replenishment and rejuvenation at Valles and Lake City calderas. *Bull. Volcanol.* **74**, 1833–1847 (2012).
35. P.W. Lipman, 2000. Calderas. In: Sigurdsson, H. (Ed.), *Encyclopedia of Volcanoes*. Academic Press, San Francisco, pp. 643– 662.
36. Z. Liu, D. Dong, P. Lundgren, Constraints on time-dependent volcanic source models at Long Valley Caldera from 1996 to 2009 using InSAR and geodetic measurements. *Geophys. J. Int.* **187**, 1283–1300 (2011).
37. F. Maccaferri, M. Bonafede, E. Rivalta, A quantitative study of the mechanisms governing dike propagation, dike arrest and sill formation. *J. Volcanol. Geotherm. Res.* **208**, 39–50 (2011).
38. F. Maccaferri, E. Rivalta, D. Keir, V. Acocella, Off-rift volcanism in rift zones determined by crustal unloading. *Nat. Geosci.*, 23–26 (2014).
39. L. G. J. Montési, 2001. Concentric dikes on the flanks of Pavonis Mons: Implications for the evolution of martian shield volcanoes and mantle plumes. In: Ernst, R.E., Buchan, K.L. (Eds.), *Mantle Plumes: Their Identification through Time*. Boulder, Colorado. In: Spec. Pap., Geol. Soc. Am., vol. **352**, pp. 165–181. T.
40. Muller, G. Ito, S. Martel, Effects of volcano loading on dike propagation in an elastic half-space. *J. Geophys. Res.* **B6, 11**, 101-111 (2001).

41. A.C. Munro, S. K. Rowland, Caldera morphology in the western Galapagos and implications for volcano eruptive behavior and mechanisms of caldera formation. *J. Volcanol. Geotherm. Res.* **72**, 85–100 (1996).
42. E. Nordlie, Morphology and Structure of the Western Galápagos Volcanoes and a Model for Their Origin. *Geol. Soc. Am. Bull.* **84**, 2931 – 2956 (1973).
43. N. Petford, a R. Cruden, K. J. McCaffrey, J. L. Vigneresse, Granite magma formation, transport and emplacement in the Earth’s crust. *Nature.* **408**, 669–673 (2000).
44. V. Pinel, C. Jaupart, The effect of edifice load on magma ascent beneath a volcano. *Philos. Trans. R. Soc. A Math. Phys. Eng. Sci.* **358**, 1515–1532 (2000).
45. M. P. Poland, A. Miklius, A. Jeff Sutton, C. R. Thornber, A mantle-driven surge in magma supply to Kīlauea Volcano during 2003–2007. *Nat. Geosci.* **5**, 295–300 (2012).
46. A. Simkin, K. Howard, Caldera Collapse in the Galapagos Islands , 1968. *Science (80)* **169**, 429–437 (1970).
47. T. Simkin, Geology of Galapagos. *Biol. J. Linn. Soc.*, 61–75 (1984).
48. T. Thordarson, S. Self, The Laki (Skaftdr Fires) and Grimsvotn eruptions in 1783-1785. *Bull. Volcanol.* **55**, 233–263 (1993).
49. L. Vezzoli, V. Acocella, Easter Island, SE Pacific: An end-member type of hotspot volcanism. *Geol. Soc. Am.* **121**, 5/6 869–886 (2009).
50. T. Watanabe, T. Masuyama, K. Nagaoka, T. Tahara, Analog experiments on magma-filled cracks: Competition between external stresses and internal pressure. *Earth Planets Space*, **54**, 1247–1261 (2002).
51. S. Yun, P. Segall, H. Zebker, Constraints on magma chamber geometry at Sierra Negra Volcano, Galápagos Islands, based on InSAR observations. *J. Volcanol. Geotherm. Res.* **150**, 232–243 (2006).
52. A. Zollo *et al.*, Seismic reflections reveal a massive melt layer feeding Campi Flegrei caldera. *Geophys. Res. Lett.* **35**, L12306 (2008).

Acknowledgements:

Constructive reviews from A. Gudmundsson, S. Burchardt and editor T. Mather significantly improved the paper. We also thank E. Holohan and M. Nikkhoo for fruitful discussions. This work was funded by the European Union through the ERC StG CCMP-POMPEI, grant agreement N. 240583, and the Supersite MED-SUV project, grant agreement N. 308665. V.A. was supported by the Italian project DPC-INGV on eruptive precursors. M.B. was supported by the European Community’s Seventh Framework Programme Grant No. 308377 (Project FUTUREVOLC) and from the Natural Environment Research Council through the Centre for the Observation and Modeling of Earthquakes, Volcanoes and Tectonics (COMET).

Figures and Legends:

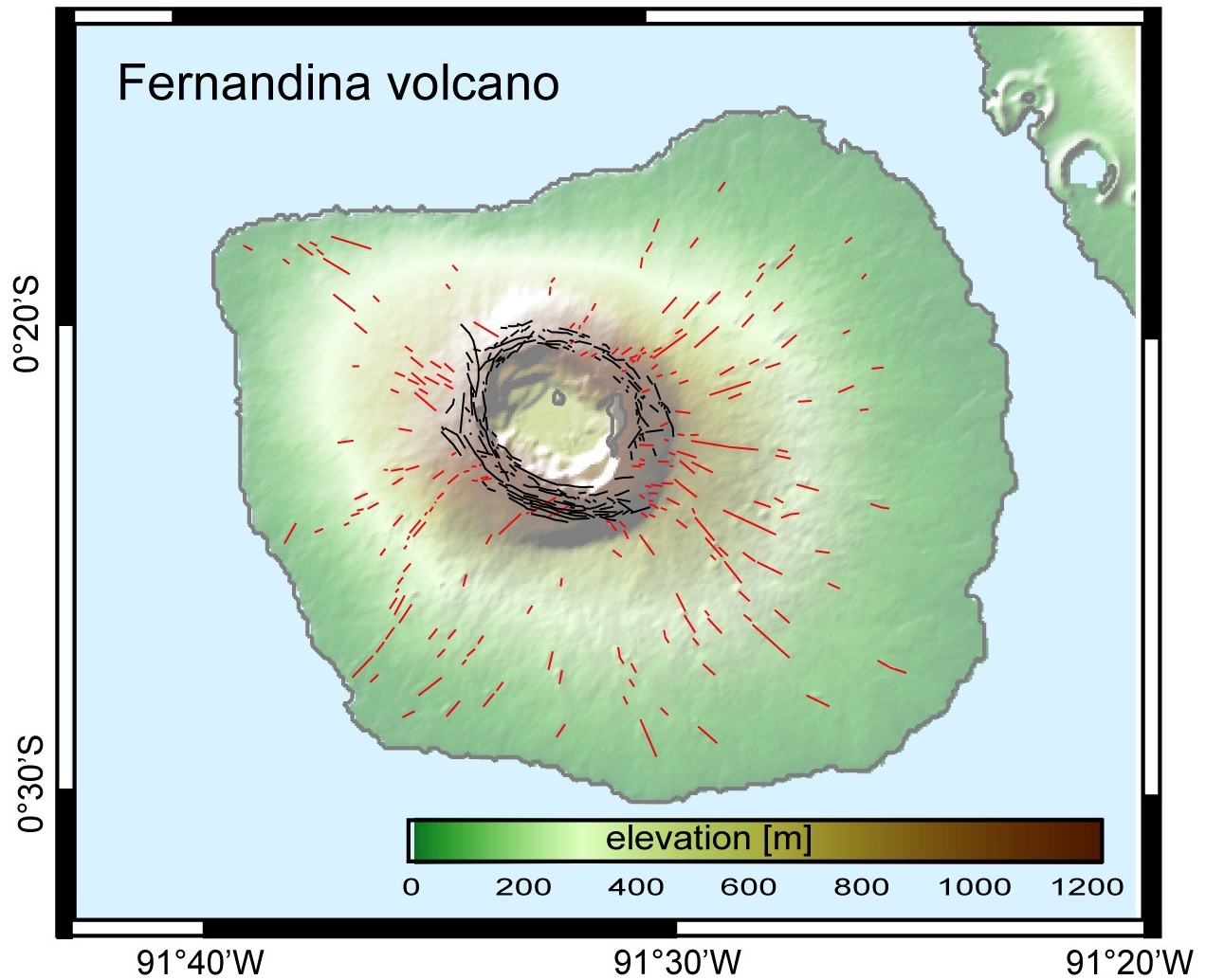


Figure 1. Shaded relief map of Fernandina with colorcoded elevation (digital elevation model from SRTM V2_1). Circumferential and radial fissures (Chadwick and Howard, 1991) are highlighted by the black and red solid lines, respectively.

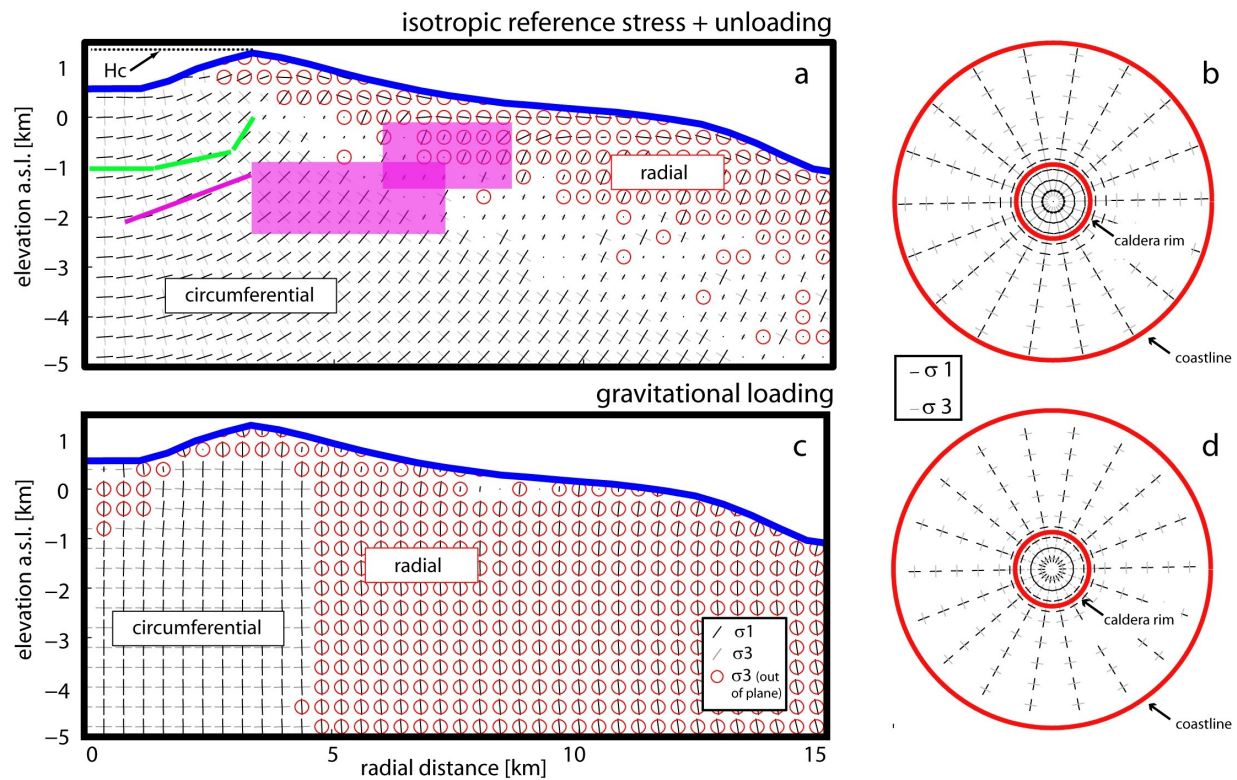


Figure 2. FE modeling results for an isotropic edifice subject to unloading (panels a and b) and gravitationally loaded (panels c and d). Panels a and c refer to the axisymmetric plane projection while panels b and d represent the map view calculated at 0 m a.s.l. H_c highlights the elevation of the caldera rim. The green lines and purple line and polygons in panel a represent the projections on the axisymmetric plane of dikes feeding the 2005 and 2009 eruptions (Chadwick et al., 2011; Bagnardi et al., 2013), respectively.

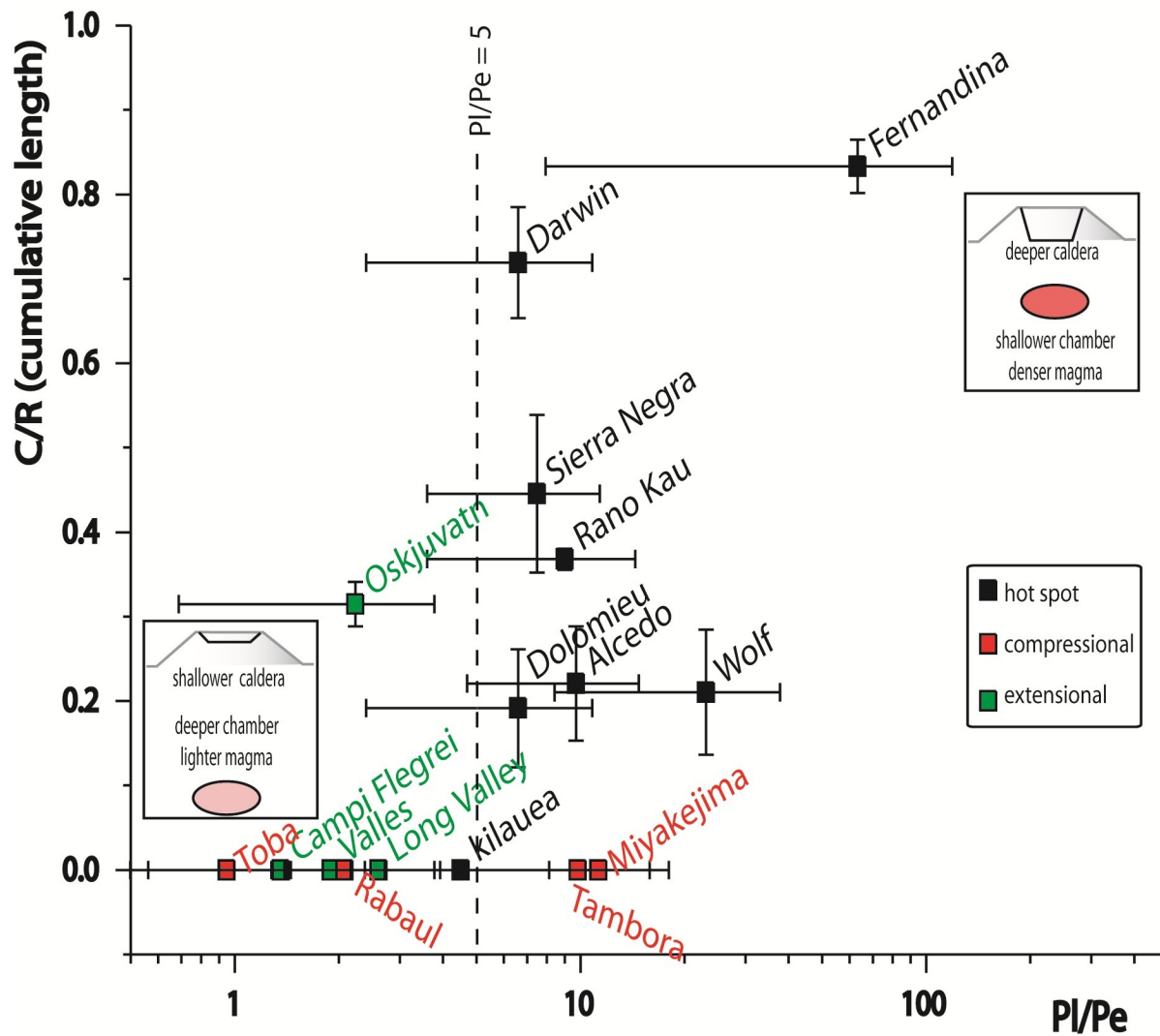


Figure 3. Cumulative length of circumferential fissures relative to that of radial ones C/R as a function of PI/Pe at well-known calderas worldwide. The loading pressure, PI , depends on the topographic difference between the average caldera rim and caldera floor. The magma overpressure, Pe , depends on the density contrast between the magma and the host rock (here assumed in the $100\text{-}300\text{ kg m}^{-3}$ for basaltic magmas and $500\text{-}700\text{ kg m}^{-3}$ for gas-rich felsic magmas) and the likely nucleation depth of the dike feeding the fissure (table ST1). Errorbars represent the depth range of magma chambers and constrain error in digitalization of fissure distribution maps (Chadwick and Howard, 1991; Carter et al., 2006; Vezzoli and Acocella 2009; Hartley and Thordarson, 2011).

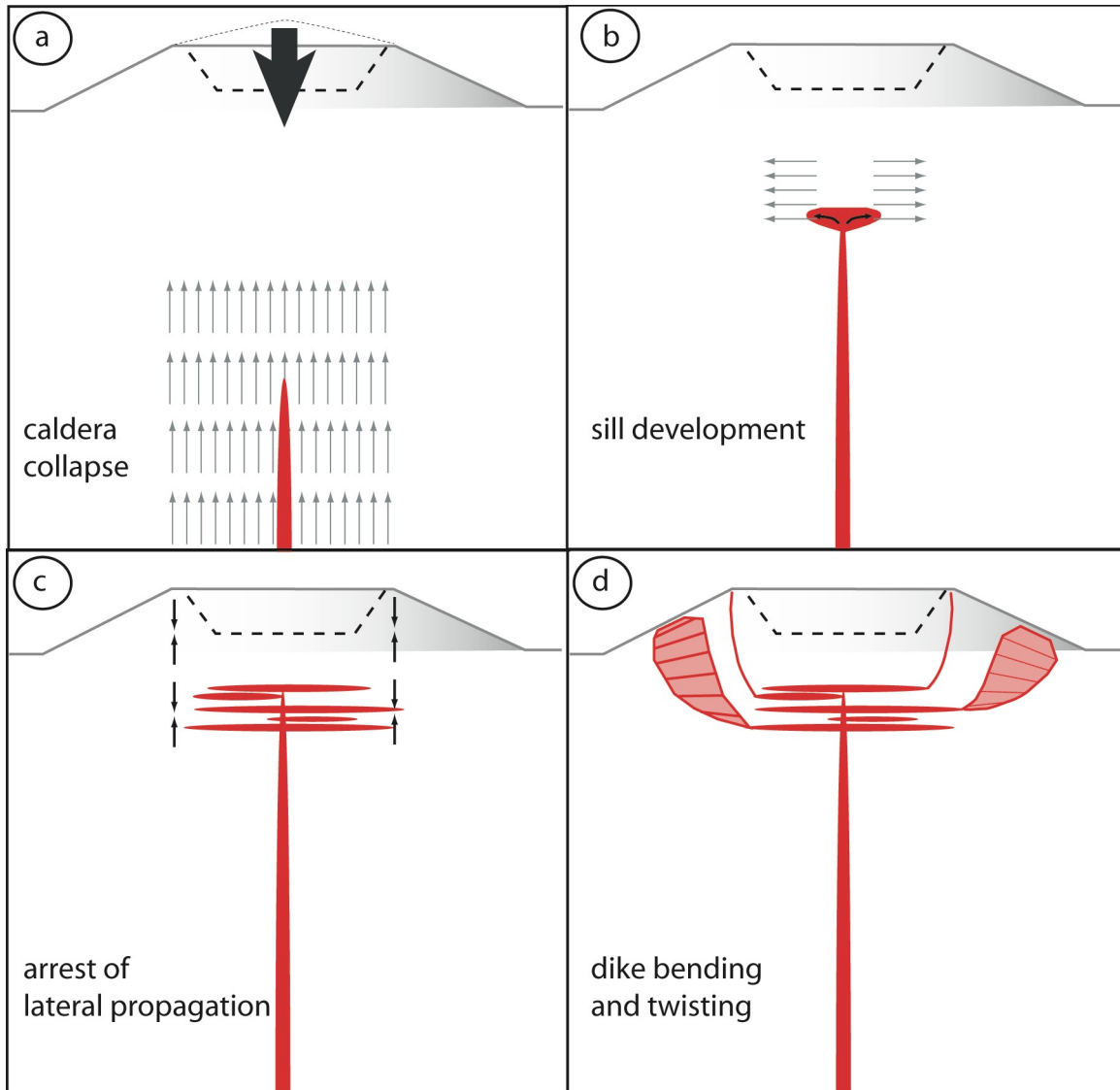


Figure 4. Four-stages evolution of the magma plumbing system associated with caldera collapse. Gray arrows indicate the principal magma (highlighted in red) propagation direction. Black arrows indicate the location of lateral propagation arrest.